Title: Graphene oxide decorated with fullerenol nanoparticles for highly efficient removal of Pb(II) ions and ultrasensitive detection by total-reflection X-ray fluorescence spectrometry

Author: Rafał Sitko, Marcin Musielak, Maciej Serda, Ewa Talik, Anna Gagor, Beata Zawisza, Małgorzata Małecka

Citation style: Sitko Rafał, Musielak Marcin, Serda Maciej, Talik Ewa, Gagor Anna, Zawisza Beata, Małecka Małgorzata. (2021). Graphene oxide decorated with fullerenol nanoparticles for highly efficient removal of Pb(II) ions and ultrasensitive detection by total-reflection X-ray fluorescence spectrometry. "Separation and Purification Technology" (2021), Vol. 277, art. no. 119450, s. 1-11. DOI: 10.1016/j.seppur.2021.119450

Separation and Purification Technology 277 (2021) 119450

Contents lists available at ScienceDirect

Separation and Purification Technology

journal homepage: www.elsevier.com/locate/seppur

Graphene oxide decorated with fullerenol nanoparticles for highly efficient removal of Pb(II) ions and ultrasensitive detection by total-reflection X-ray fluorescence spectrometry

Rafal Sitko [a,*], Marcin Musielak [a], Maciej Serda [a], Ewa Talik [b], Anna Gagor [c], Beata Zawisza [a], Malgorzata Malecka [c]

[a] Institute of Chemistry, University of Silesia, Szkolna 9, 40-006 Katowice, Poland
[b] Institute of Physics, University of Silesia, 75 Pulku Piechoty 1, 41-500 Chorzow, Poland
[c] Institute of Low Temperature and Structure Research, Polish Academy of Science, P.O. Box 1410, 50-950 Wroclaw, Poland

ARTICLE INFO

Keywords:
Hydroxyfullerene
Fullerol
Fullerene
Preconcentration
Removal

ABSTRACT

In this paper, the graphene oxide (GO) decorated with fullerenol nanoparticles $C_{60}(OH)_{22}$ has been designed for the highly selective separation and ultrasensitive determination of lead ions. The grafting fullerenol nanoparticles to the surface of GO solves the problem of their high solubility in aqueous solutions and simultaneously uses their high hydrophilicity and deprotonation ability. The research has revealed unique adsorption properties of GO-$C_{60}(OH)_{22}$ toward Pb(II) ions at pH 5.5, i.e., minimal adsorbent dose (5 mg L^{-1}), impressive resistance to ionic strength (up to 1 mol L^{-1}), and enormous adsorption capacity (1307 mg g^{-1}), much higher than those of any of the currently reported sorbents. The adsorption isotherms, kinetics, and effect of ionic strength indicate that an inner-sphere model based on surface complexation is the main mechanism of Pb(II) adsorption on GO-$C_{60}(OH)_{22}$. The high-resolution O1s and Pb4f X-ray photoelectron spectra confirm the strong chelation of Pb(II) ions and suggest the various coordination of Pb(II) ions to the oxygen functional groups. The exceptional properties of GO-$C_{60}(OH)_{22}$, including the possibility of application in micro-quantities, were the basis for the development of the method for ultra-sensitive detection of Pb(II) ions using such micro-analytical technique as total-reflection X-ray fluorescence spectrometry (TXRF). The method allows obtaining an extremely low detection limit of 2.3 pg mL^{-1} using a low-power TXRF instrument. Due to the impressive selectivity of the method, the ultra-trace Pb(II) ions can be highly accurately determined in complex matrix samples, including high salinity waters challenging to analyze using other analytical techniques.

1. Introduction

The anthropogenic emission of lead into the environment draws particular attention in the view of green chemistry due to its high hazardousness, even at low concentrations. Regular or even short exposures to lead severely increase the risk of its bioaccumulation in human internal organs [1], thus causing malfunctions in their proper function or even leading to their failure since it affects the enzymatic activity [2,3]. Unfortunately, industrial wastes commonly pollute the groundwater, which creates an additional risk of lead getting into drinking water and food [4]. According to EPA regulations [5], the maximum contaminant level (MCL) of lead in drinking water is set to 15 ng mL^{-1}, but the maximum contaminant level goal (MCLG), below which there is no known or expected risk to human health, equals zero. Hence the need to develop highly effective methods for lead removal from aqueous solutions and ultra-sensitive lead determination methods. The most frequently used techniques in the determination of Pb(II) are flame atomic absorption spectrometry (FAAS) [6,7], inductively coupled plasma optical emission spectrometry (ICP-OES) [8–10], and very sensitive electrothermal atomic absorption spectrometry (ET-AAS) [11–13] or inductively coupled plasma mass spectrometry (ICP-MS) [14–16]. However, the direct determination of ultra-trace Pb(II) ions using these techniques can be seriously hampered because of their insufficient sensitivity (especially FAAS) and/or matrix interferences. Therefore, the preconcentration/separation step can be required to determine trace and ultra-trace Pb(II) in complex matrix samples. In recent years, the

* Corresponding author.
E-mail address: rafal.sitko@us.edu.pl (R. Sitko).

https://doi.org/10.1016/j.seppur.2021.119450
Received 5 July 2021; Received in revised form 4 August 2021; Accepted 5 August 2021
Available online 8 August 2021

most frequently used sample pretreatment techniques are liquid–liquid microextraction (LLME) [9,12], and methods based on solid-phase extraction (SPE) such as solid-phase microextraction (SPME) [15], dispersive micro-solid phase extraction (DMSPE) [6,10], and magnetic dispersive solid-phase extraction (MDSPE) [8,13,16]. The rapid development of micro-extraction techniques (SPME, DMSPE, MDSPE) was largely possible due to new materials with interesting adsorptive properties.

The carbon nanomaterials and their adsorptive properties have drawn significant attention from the scientific community in recent years. Most research concerns the use of carbon nanotubes, graphene, their chemical modification, and especially graphene oxide due to its impressive adsorption capacity toward metal ions [17–21]. Many articles are devoted to the removal and determination of lead ions using nanomaterials [22,23]. Extensive research in this area results from the high toxicity of this metal and many Pb contamination sources, making it a problem on a global scale. However, a limited number of publications concern fullerenes, discovered already in 1985 [24]. Fullerene C_{60}, the most popular of fullerenes, has a spherical structure composed of a fused ring polycyclic system with 20 six- and 12 five-membered rings. Fullerene C_{60} is slightly soluble in some nonpolar organic solvents such as toleune and practically insoluble in water. Due to the lack of functional groups with donor atoms, fullerenes are interesting in the adsorption of organic compounds rather than metal ions (unless the metal species are converted to neutral chelates) [25–29]. However, unlike the other two carbon allotropes like graphite and diamond, fullerene is much more reactive. As an electron-deficient alkene, fullerene C_{60} readily reacts with electron-rich species [30]. Therefore, fullerene can be chemically functionalized by attaching various functional groups to improve its solubility and adsorptive properties. Some reports suggest using hexakis-substituted fullerene C_{60} adducts as scaffolds to prepare metal–organic frameworks by coordinating ruthenium or zinc ions [31,32]. Several structures based on fullerenes covalently attached to metal-chelating groups (porphyrins, pyridine, bipyridine, phenanthroline, crown ethers, etc.) have also been developed [33]. These materials are promising components in artificial photosynthetic. Unfortunately, the solubility of these systems is still limited, and chelating centers are not available for metal ions present in an aqueous solution. However, the almost complete insolubility of fullerene C_{60} can be easily overcome by a simple hydroxylation reaction. Polyhydroxylated fullerenes $C_{60}(OH)_n$, so-called fullerols, fullerenols, or hydroxyfullerenes were first synthesized by Chiang *et al.* by the reaction of fullerene with sulphuric/nitric acids [34] or by the hydrolysis of the esters of a polyhydroxy organo-carboxylated C_{60} fullerene [35]. Several methods for the synthesis of fullerenols with the various number of hydroxyl groups have been reported since 1992 [30]. However, the simplest and most frequently used method for the synthesis of fullerenols is the direct reaction of fullerene with sodium hydroxide in the presence of quaternary ammonium cations proposed by Li *et al.* [36]. The solubility of fullerenols $C_{60}(OH)_n$ in water is excellent and depends on degrees of hydroxylation ($2 \leq n \leq 42$), e.g. 17.5 and 58 mg mL^{-1} for $C_{60}(OH)_{36}$ and $C_{60}(OH)_{40}$, respectively [37] (for comparison, the solubility of C_{60} in water is equal to 1.3×10^{-11} mg mL^{-1}) [38]. In aqueous solutions, depending on the pH, fullerenols are more or less deprotonated, and due to their agglomeration, they form clusters that are still highly soluble in water [39,40]. Anderson and Barron reported that soluble fullerenol reacts with metal ions to produce insoluble metal-fullerenol cross-linked polymers [41]. The authors proposed that the fullerenol acts as a chelate ligand to the metal ions and can be used to remove metal ions *via* precipitation [41,42]. However, the precipitation time strongly depends on metal concentration. The fullerenol remains soluble in water if the concentration of metal ions is very low. Thus, the application of pure fullerenol in trace or ultra-trace separation is limited.

This paper shows that the surprising complexing properties of fullerenol toward metal ions and its high hydrophilicity can be exploited in ultra-trace inorganic analysis. Moreover, the problem of the high solubility of fullerenes, also in the presence of trace amounts of metal ions, can be solved by grafting $C_{60}(OH)_{22}$ nanoparticles to the surface of graphene oxide (GO). The research has revealed that the nano-adsorbent GO-$C_{60}(OH)_{22}$ has unique adsorption properties towards Pb(II) ions. Huge adsorption capacity, impressive selectivity toward Pb(II) ions, and excellent dispersibility in aqueous solutions made it possible to use GO-$C_{60}(OH)_{22}$ for highly efficient removal of Pb(II) ions from aqueous solution. Moreover, these features opened the path to a simple and ultra-sensitive Pb(II) determination by such micro-analytical technique as total-reflection X-ray fluorescence spectrometry (TXRF). This work shows that the detection limits at the ppt level can be obtained using the simple micro-analytical approach.

2. Experimental section

2.1. Reagents

Fullerene C_{60}, 99.5% (SES Research, Houston, TX, USA); Amberlist-15 (POCh, Gliwice, Poand); toluene, 4-Dimethylaminopyridine DMAP, and 1-ethyl-3-(3-dimethylaminopropyl)carbodiimide hydrochloride EDCI (Sigma-Aldrich, St. Louis, MO, USA); tetrabutylammonium hydroxide Bu_4NOH (Acros Organics, Antwerp, Belgium); cellulose membranes (Spectrum Labs, San Francisco, California, USA); Lead standard solution (Merck Certipur®, Darmstadt, Germany); metal salts, sodium nitrate, nitric acid and sodium hydroxide p.a. class (POCh, Gliwice, Poland); 0.45 μm pores nitrocellulose membranes discs (Merck Millipore, Molsheim, France); Certified reference materials: Spring water NIST 1640a (National Institute of Standards and Technology, Gaithersburg, Maryland, USA); Ground water BCR-610 (JRC - Joint Research Centre, Geel, Belgium); Estuarine water LGC 6016 (LGC Standards GmbH, Wesel, Germany); Sea water QC3163 (Sigma-Aldrich, St. Louis, MO, USA); High purity water: Milli-Q system (Millipore, Molsheim, France).

2.2. Instruments

Total-reflection X-ray fluorescence spectrometry (TXRF): S4 T-STAR spectrometer (Bruker AXS Microanalysis GmbH, Berlin, Germany) equipped with Mo target X-ray tube of 50 W operating at 50 kV and 1000 μA, silicon drift detector, and multilayer monochromator; Energy-dispersive X-ray fluorescence spectrometry (EDXRF): Epsilon 3 spectrometer (Malvern Panalytical, Almelo, Netherlands) equipped with Rhodium target X-ray tube of a 50 μm Be window with maximum power of 9 W (measurements conditions: 30 kV, 300 μA, 100 μm Ag primary beam filter, 300 s counting time, air atmosphere); Inductively coupled plasma optical emission spectrometry (ICP-OES): Spectroblue spectrometer (Spectro Analytical Instruments GmbH, Germany); Scanning electron microscopy (SEM): JEOL-7600F instrument with the Oxford X-ray energy-dispersive spectrometer (Akishima, Tokyo, Japan); Transmission electron microscopy (TEM): CM-20 SuperTwin instrument operating at 160 kV (Philips, Amsterdam, Netherlands); X-ray photoelectron spectroscopy (XPS): PHI 5700/660 spectrometer supplied with the monochromated Al K_α radiation source (Chanhassen, Minnesota, USA); Fourier-transform infrared spectroscopy (FT-IR): Nicolet iS50 FT-IR spectrometer (Thermo Fisher Scientific, Waltham, Massachusetts, USA). The KBr pellets composed of 200 mg KBr and 1 mg of GO or $C_{60}(OH)_{22}$ or GO-$C_{60}(OH)_{22}$ were measured in the range of 4000–400 cm^{-1}.

2.3. Synthetic procedure for GO-$C_{60}(OH)_{22}$

To synthesize GO-fullerenol hybrid GO-$C_{60}(OH)_{22}$, a water-soluble C_{60} fullerene derivative $C_{60}(OH)_{22}$ was prepared first using a modified procedure reported earlier by Heimann et *al.* [42]. Additionally, to ensure that the prepared fullerene nanomaterial would not possess incorporated sodium cations, (-ONa groups), we used polystyrene-based

ion exchange resin Amberlist15 (H^+ form) in the purification process. Briefly, C_{60} (360 mg, 0.50 mmol) was dissolved in a dry toluene (300 mL) and treated with 200 mL of a concentrated solution of NaOH (12.5 M). After stirring at room temperature for 30 min, 0.5 mL of Bu_4NOH was added to the reaction mixture. Fifteen minutes later, the organic layer became transparent, and the reaction mixture was stirred at room temperature for an additional 1 h. After that time, the toluene phase was removed using a pipette, stirred for additional 48 h, and then 5 mL of methanol were added. The brown fullerenol solid was collected and dissolved again in ultrapure water with the addition of 1 g of Amberlist 15, stirred for two hours, finally dialyzed using a cellulose membrane (molecular weight exclusion limit 1.0 kDa; Spectrum Labs, CA, USA), and then lyophilized. The pure fullerene nanomaterial was then ready to be conjugated with GO (synthesized by the modified Hummers' method [43], and characterized in our previous paper [44]). The conjugation process was performed by sonification of 100 mg of GO in 100 mL of ultrapure water for 30 min (temperature of GO solution did not exceed 50 °C) and then treating the solution with a mixture of DMAP (122 mg, 1 mmol) and EDCI hydrochloride (380 mg, 2 mmol). To the activated GO water suspension, 100 mg of fullerenol was added and the reaction mixture was stirred for additional 48 h at room temperature. The obtained GO-fullerenol hybrid was resuspended three times in ultrapure water and centrifuged for 30 min at 5000 rpm. The final solid of GO-$C_{60}(OH)_{22}$ was dried for 5 h. The purity of synthesized GO-$C_{60}(OH)_{22}$ was verified by XPS and EDXRF. The XPS spectra revealed only the presence of carbon and oxygen, confirming that DMAP, EDCI and their products were removed during the purification process. The EDXRF spectra confirmed that GO-$C_{60}(OH)_{22}$ is not contaminated with heavy metals. In the preconcentration and determination of Pb(II) ions, the suspension of GO-$C_{60}(OH)_{22}$ was used. The suspension of concentration 1 mg mL^{-1} was prepared by ultrasonication of 25 mg of GO-$C_{60}(OH)_{22}$ in 25 mL of high-purity water for 60 min.

2.4. Batch adsorption experiment

GO-$C_{60}(OH)_{22}$ was dispersed in 20 mL of Pb(II) aqueous solutions. Then, the pH of the suspension was adjusted with nitric acid and/or sodium hydroxide solutions. The suspension was stirred (900 rpm) for 180 min to achieve adsorption equilibrium. The suspensions were filtered through a 0.45 μm membrane filter. The concentration of Pb(II) ions in filtrate (C_e, mg L^{-1}) was determined by ICP-OES. The amount of Pb(II) adsorbed on GO-$C_{60}(OH)_{24}$ (q_e, mg g^{-1}) was measured using EDXRF spectrometry. Specific experimental conditions are given in brackets: effect of pH (pH 1–8, 5 mg L^{-1} of GO-$C_{60}(OH)_{22}$, 250 ng mL^{-1} of Pb(II), adsorption time 180 min), kinetics (pH 5.5, 1 and 5 mg L^{-1} of GO-$C_{60}(OH)_{22}$, 100 and 500 ng mL^{-1} of Pb(II), adsorption time 5–180 min), adsorption isotherms (pH 5.5, 5 mg L^{-1} of GO-$C_{60}(OH)_{22}$, 0.25–100 mg L^{-1} of Pb(II), adsorption time 180 min), effect of ionic strength (pH 5.5, 5 mg L^{-1} of GO-$C_{60}(OH)_{24}$, 50 ng mL^{-1} of Pb(II), adsorption time 180 min, 0.001–5 mol L^{-1} of $NaNO_3$), effect of coexisting ions (pH 5.5, 5 mg L^{-1} of GO-$C_{60}(OH)_{22}$, 25 ng mL^{-1} of Pb(II), adsorption time 60 min), desorption and reusability studies (pH 5.5, 5 mg L^{-1} of GO-$C_{60}(OH)_{22}$, 10 μg mL^{-1} of Pb(II), adsorption time 180 min, 0.1 M HNO_3 as eluent).

2.5. Determination of Pb(II) ions using GO-$C_{60}(OH)_{22}$ and TXRF

The preconcentration of Pb(II) ions was performed using DMSPE: 500 μL of GO-$C_{60}(OH)_{22}$ suspension (1 mg mL^{-1}) was injected into the analyzed solution of volume up to 100 mL. The pH of the sample was adjusted to 5.5 with nitric acid and sodium hydroxide solutions, and the sample was stirred for 30 min. After the adsorption step, the GO-$C_{60}(OH)_{22}$ with adsorbed Pb(II) ions was isolated from the solution by filtration using nitrocellulose membrane with 0.45 μm pores (Merck Millipore) and a filtration assembly with a diameter of 5 mm. Next, the membrane loaded with GO-$C_{60}(OH)_{22}$ was placed in 1.5 mL Eppendorf containing 0.5 mL of 1 μg mL^{-1} of Y internal standard in 1 mol mL^{-1} HNO_3. Subsequently, the GO-$C_{60}(OH)_{22}$ was dispersed by ultrasonication for 2 min. Finally, 10 μL suspension was pipetted on a siliconized quartz reflector, dried on a hotplate at 50 °C for 5 min, and measured by TXRF.

3. Results and discussion

3.1. Characterization of GO-$C_{60}(OH)_{22}$

The fullerenol nanoparticles $C_{60}(OH)_{22}$ were covalently bonded to GO nanosheets by coupling the hydroxyl groups of $C_{60}(OH)_{22}$ and the carboxyl groups of GO using EDCI as a coupling reagent and DMAP as the catalyst. The SEM image shows the wrinkled nano-flakes of synthesized GO-$C_{60}(OH)_{22}$ (Fig. 1a), but only the TEM images revealed the presence of $C_{60}(OH)_{22}$ particles on the surface of transparent GO nanosheets (Fig. 1b). The nanoparticles visible on the GO nanosheets are a few nm in size and do not exceed 10 nm. Their diameter is larger than the size of a single fullerenol molecule, i.e., 1.2 nm. It suggests that due to the aggregation $C_{60}(OH)_{22}$ formed clusters of a few nanometers in size. Such aggregation of the fullerenol nanoparticles, even at low pH, was demonstrated using flow field-flow fractionation and atomic force microscopy by Assemi *et al.* [39]. Fig. 1c shows the FT-IR spectra of GO, $C_{60}(OH)_{22}$ and GO-$C_{60}(OH)_{22}$. Both GO, and $C_{60}(OH)_{22}$ spectra are characteristic for graphene oxide [45–48] and hydroxyfullerene [49–51]. Intense and very broad bands around 3500 cm^{-1} confirm the presence of O-H stretching vibrations from C-OH groups and intercalated H_2O particles. In $C_{60}(OH)_{22}$ three broad peaks may be assigned to stretching C═C (1650 cm^{-1}), bending δCOH and δOH (at ca. 1370 cm^{-1}), and stretching hydroxy C-OH (1090 cm^{-1}) vibrations. In GO, an additional strong band near 1720 cm^{-1} comes from stretching C═O vibrations of carbonyl and carboxyl groups. Towards lower wavelengths, there is an area of C═C valence bends (1500–1650 cm^{-1}) and further C-O vibrations from various groups (δ(COH) bending modes ~ 1370 cm^{-1}, stretching C-O in the region 1310–1000 cm^{-1} with two pronounced peaks that may be assigned to carboxyl groups (~1240 cm^{-1}) as well as C-O-C and hydroxy C-OH stretching (~1060 cm^{-1})). There is also evidence of out-of-plane γ(COH) bending (960–880 cm^{-1}). The spectrum of GO-$C_{60}(OH)_{22}$ shows qualitative changes compared to the used substrates, which confirm the chemical modification of GO. In the region of C-O stretching a new maximum arises at approx. 1200 cm^{-1} that may be attributed to vibrations of ester bridges. The band around 1060 cm^{-1} decreases meaningfully which points to the reduction of the C-O-C and C-OH vibrations. The GO and GO-$C_{60}(OH)_{22}$ were also characterized by X-ray photoelectron spectroscopy (XPS). The C1s spectrum of GO (Fig. 1d) shows the main peak at 284.6 eV assigned to the non-oxidized carbon C-C/C-H and four peaks at 285.9, 287.0, 288.2, 289.5 eV assigned to oxidized carbon, i.e., C-OH, C-O-C, C═O, and O-C═O, respectively. The C1s spectrum of GO-$C_{60}(OH)_{22}$ reveals the same peaks of non-oxidized carbon at 286.7 eV and oxidized carbon, i.e., C-OH, C-O-C, C═O, and O-C═O, slightly shifted to lower energy at 285.7, 286.7, 287.8, 288.8 eV. The fullerenol usually reveals the peaks at 284.7–284.8 eV assigned to the non-oxidized carbon, mono-oxidized carbon (C-OH) at 284.8–286.7 eV, and di-oxidized carbon (C═O) or deprotonated hydroxyl groups (C-O^-) at 286.7–288.3 eV [50,52–54]. After the chemical attachment of $C_{60}(OH)_{22}$ to GO, a change in intensities of C-OH, C-O-C, C═O peaks can be observed. Moreover, the peak of the carboxyl group at 289.5 eV of GO is shifted to lower binding energy (288.8 eV), indicating the ester linkage and chemical attachment of $C_{60}(OH)_{22}$ to GO nanosheets [55]. The O1s spectrum of GO (Fig. 1e) reveals three peaks at 531.2, 532.7, and 534.0 eV assigned to C═O (carboxyl and carbonyl groups), C-OH/C-O-C (hydroxyl and epoxy groups), and H_2O/C-OH (carboxyl group), respectively [56–58]. The O1s spectrum of GO-$C_{60}(OH)_{22}$ shows the same peaks at similar binding energies (531.3, 532.8, and 534.2 eV) but, similar to the C1s spectrum, the different ratio in their intensities.

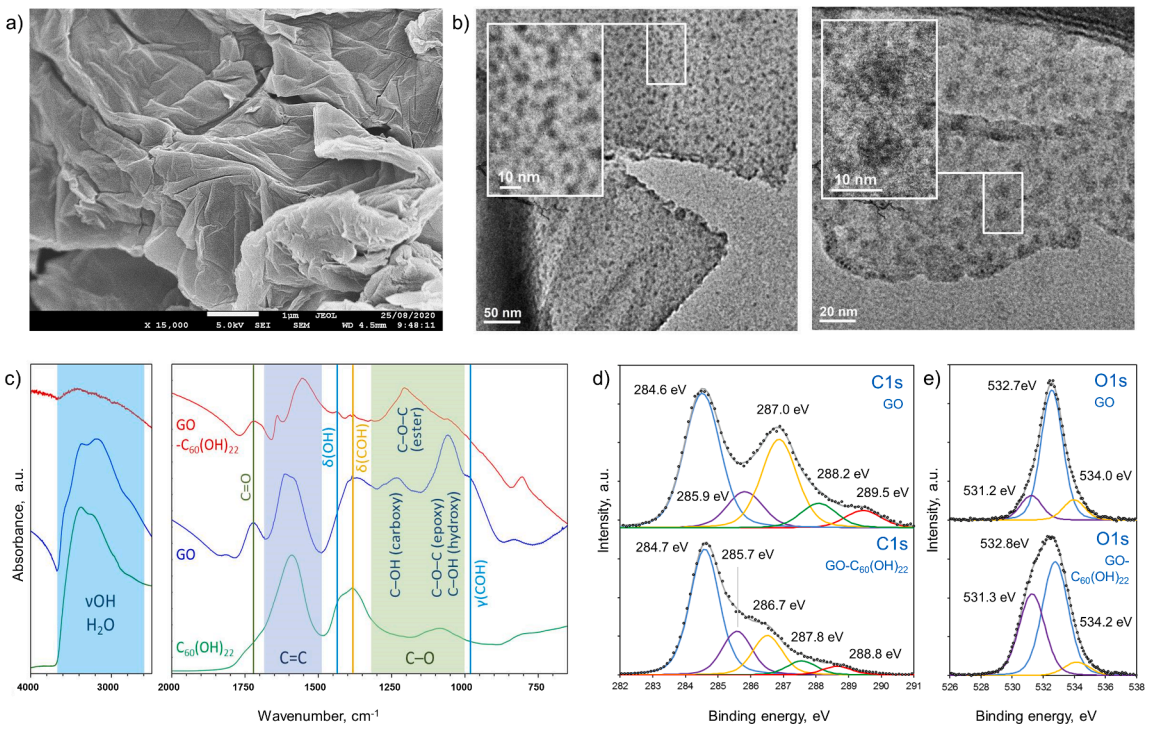

Fig. 1. Characterization of GO-$C_{60}(OH)_{22}$: (a) SEM and (b) TEM images of the GO-$C_{60}(OH)_{22}$, (c) FT-IR spectra of GO, $C_{60}(OH)_{22}$ and GO-$C_{60}(OH)_{22}$ (ν – stretching vibrations, δ – in-plane bending (scissoring), γ – out-of-plane bending), and (d, e) high-resolution XPS C1s and O1s spectra of GO and GO-$C_{60}(OH)_{22}$.

3.2. Adsorption of Pb(II) ions on GO-$C_{60}(OH)_{22}$

In this work, GO-$C_{60}(OH)_{22}$ was synthesized by coupling the carboxyl groups of GO and the hydroxyl groups of $C_{60}(OH)_{22}$ using water-soluble carbodiimide EDCI and DMAP catalyst. Therefore, it can be assumed that the majority of carboxyl groups of GO bounded to $C_{60}(OH)_{22}$ are unavailable for the adsorption of Pb(II) ions, and only hydroxyl groups of $C_{60}(OH)_{22}$ molecules and GO nanosheets will be responsible for the adsorption. The acidity of the solution plays a crucial role in the adsorption of metal ions. Therefore, this effect was tested first. Because the acidity effect was investigated in pH range from 1 to 8, the concentration of Pb(II) ions was fixed at a low level (250 ng mL^{-1}) to prevent their precipitation (especially in basic solution) and to assure that removal of Pb(II) is based on adsorption, not precipitation. As it is shown in Fig. 2a, the acidity of the solution strongly influences the adsorption of Pb(II) ions. The adsorption of Pb(II) ions on GO-$C_{60}(OH)_{22}$ increases quickly at pH 3–5, remains constant at pH 5–6 and decreases slowly at pH 6–8. Such a relationship can be explained by the surface charge of fullerenol and GO nanoparticles, which strongly depends on pH solutions. Electrokinetic and potentiometric titration data indicate that $C_{60}(OH)_{22}$ nanoparticles are negatively charged at pH > 3, and the number of deprotonated surface sites increases with pH [39,40]:

$$GO\text{-}C_{60}(OH)_{22} + nH_2O \leftrightarrow [GO\text{-}C_{60}(OH)_{22\text{-}n}O_n]^{n-} + nH_3O^+$$

These sites are available for the adsorption of Pb(II) cations *via*

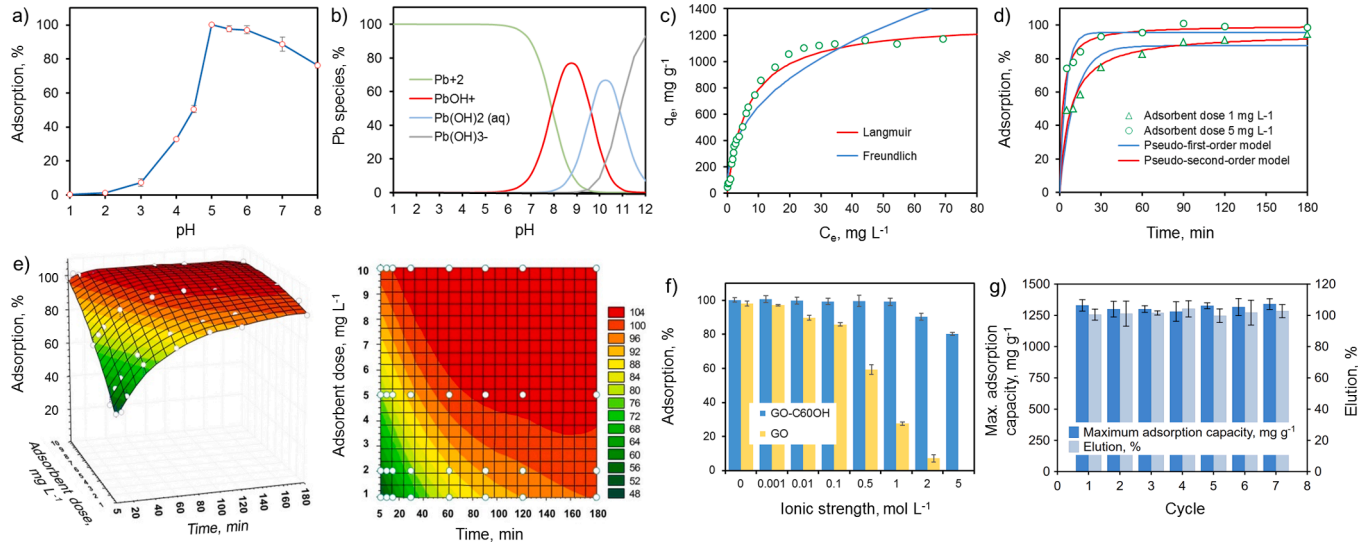

Fig. 2. Influence of pH on adsorption of Pb(II) on GO-$C_{60}(OH)_{22}$ (a), Pb(II) species at different pH (b), Langmuir and Freundlich isotherms of Pb(II) adsorption on GO-$C_{60}(OH)_{22}$ (c), kinetics of Pb(II) adsorption on GO-$C_{60}(OH)_{22}$ (d), effect of adsorbent time and adsorbent dose (e), influence of ionic strength on Pb(II) adsorption on GO-$C_{60}(OH)_{22}$ and GO (f), reuse of GO-$C_{60}(OH)_{22}$ (g).

electrostatic interactions. However, the chelation of Pb(II) ions by deprotonated hydroxyl groups is also possible. Anderson and Barron proposed that the fullerenol could act as a chelate ligand to the metal ions [41]. For the divalent metal ions, both the 1,2-diol (similar to metal–catechol coordination mode) and 1,3-diol coordination are possible [42]. As shown in Fig. 2b, Pb(II) ions are present as Pb^{2+} species at pH < 6. Therefore, the complexation reaction can be written as follows:

$$[GO\text{-}C_{60}(OH)_{22\text{-}n}O_n]^{n\text{-}} + mPb^{2+} \leftrightarrow [GO\text{-}C_{60}(OH)_{22\text{-}n}O_{n\text{-}2m}(O_2Pb)_m]^{(n\text{-}2m)\text{-}}$$

The decreasing Pb(II) adsorption at pH above 6 can be explained by the gradual formation of the hydroxide complex $Pb(OH)^+$ (Fig. 2b) and the chemical equilibrium that established between $Pb(OH)^+$ species and Pb(II) ions adsorbed on GO-$C_{60}(OH)_{22}$. If the pH is increased above 6, the equilibrium shifts to the left, and the adsorption of Pb(II) ions decrease according to equilibrium:

$$[GO\text{-}C_{60}(OH)_{22\text{-}n}O_n]^{n\text{-}} + mPb(OH)^+ \leftrightarrow [GO\text{-}C_{60}(OH)_{22\text{-}n}O_{n\text{-}2m}(O_2Pb)_m]^{(n\text{-}2m)\text{-}} + mOH^-$$

The adsorption of Pb(II) ions on GO-$C_{60}(OH)_{22}$ simulated using Langmuir [59,60], Freundlich [61], Elovich [62], and Temkin [63] isotherm models indicated the chemical nature of this process (Table 1). The Freundlich and Elovich models assuming multi-layer adsorption are the worst fitted to the experimental data. The best fit of the Langmuir model (see also Fig. 2c) indicates that the adsorption of Pb(II) ions is based on chemisorption, i.e., the chelation of Pb(II) ions by deprotonated hydroxyl groups. The positive variation of adsorption energy calculated from the Temkin model indicates that Pb(II) adsorption is exothermic. The favorable adsorption is also confirmed by the constant separation coefficient, which ranges from 0.06 to 0.96 for all the initial concentrations of Pb(II), i.e., it stays within the range of 0–1 [64]. The maximum adsorption capacity of GO-$C_{60}(OH)_{22}$ toward Pb(II) ions calculated from the well-fitted Langmuir model is impressive and equals 1307 mg g^{-1} (Table 1).

This value is higher than the adsorption capacity of GO (1041 mg g^{-1}) used for the synthesis of GO-$C_{60}(OH)_{22}$. The study on the kinetics of Pb(II) adsorption on GO-$C_{60}(OH)_{22}$ presented in Fig. 2d and Table 2 shows that the pseudo-second-order rate kinetic model [65] is better fitted to the experimental data than the pseudo-first-order rate model [66]. This indicates that the adsorption capacity is proportional to the number of hydroxyl groups on the GO-$C_{60}(OH)_{22}$. As can be seen, the kinetics of the adsorption process strongly depends on the dose of GO-$C_{60}(OH)_{22}$. It should be also emphasized that using a very small adsorbent dose of 5 mg L^{-1} allows achieving over 90% removal of Pb(II) ions within only 30 min (the adsorption at equilibrium calculated from the pseudo-second-order rate kinetic model is equal to 100%). The lower dose of the adsorbent (1 mg L^{-1}) results in a slower adsorption process and is insufficient to achieve 100% adsorption at equilibrium. Fig. 2e shows the dependence of Pb(II) adsorption on the adsorption time and adsorbent dose. As can be seen, the larger the adsorbent dose, the shorter the adsorption time. At a dose of 10 mg L^{-1}, the adsorption close to 100% is achieved in<5 min. The very short adsorption time with such a small adsorbent dose results from the wrinkled structure and flexibility of GO nanosheets decorated with $C_{60}(OH)_{22}$, and most of all, the excellent dispersibility in water due to the small particle size and high hydrophilicity of GO-$C_{60}(OH)_{22}$.

Table 1
Parameters of isotherm models for adsorption of Pb(II) on GO-$C_{60}(OH)_{22}$.

Isotherm model		
Langmuir	q_{max}	1307
$q_e = \frac{q_{max}K_LC_e}{1+K_LC_e}$	K_L	0.15
	R^2	0.9901
Freundlich	K_F	259.7
$q_e = K_FC_e^{1/n}$	n	2.48
	R^2	0.9080
Temkin	ΔQ	12.4
$\frac{q_e}{q_{max}} = \frac{RT}{\Delta Q}lnK_TC_e$	K_T	1.80
	R^2	0.9490
Elovich	q_{max}	479
$\frac{q_e}{q_{max}} = K_EC_e exp\left(-\frac{q_e}{q_{max}}\right)$	K_E	0.66
	R^2	0.8360
The constant separation coefficient		
$R_L = \frac{1}{1+K_LC_0}$	R_L	0.06–0.96

q_e – amount of adsorbed ions at equilibrium (mg g^{-1}), q_{max} – maximum amount of adsorbed ions (mg g^{-1}), C_e – equilibrium concentration (mg L^{-1}), K_L – Langmuir constant related to free energy of adsorption (L mg^{-1}), K_F – Freundlich constants related to the adsorption capacity ($mg^{1\text{-}n}$ L^n g^{-1}), n – Freundlich constants related to the adsorption intensity, K_T - Temkin equilibrium constant (L mg^{-1}), R – universal gas constant (J mol^{-1} K^{-1}), T – temperature (K), $\Delta Q = -\Delta H$ – variation of adsorption energy (kJ mol^{-1}), K_E – Elovich equilibrium constant (L mg^{-1}).

Table 2
Kinetic parameters of kinetic models for adsorption of Pb(II) on GO-$C_{60}(OH)_{22}$.

Kinetic model		Adsorbent dosage	
		1 mg L^{-1}	5 mg L^{-1}
Pseudo-first-order equation	q_e	87.7 ± 4.0	95.7 ± 2.7
$q_t = q_e(1-exp(-k_1t))$	k_1	0.093 ± 0.017	0.224 ± 0.031
	R	0.9668	0.9825
Pseudo-second-order equation	q_e	95.5 ± 3.4	100.0 ± 1.6
$q_t = \frac{k_2q_e^2t}{1+k_2q_et}$	k_2	0.0014 ± 0.00028	0.0046 ± 0.00071
	R	0.9873	0.9960

q_e – amount of adsorbed ions at equilibrium (mg g^{-1}), q_t – amount of adsorbed ions at time t (mg g^{-1}), k_1 – pseudo-first-order rate constant (min^{-1}), k_2 – pseudo-second-order rate constant (g mg^{-1} min^{-1}).

GO-$C_{60}(OH)_{22}$ exhibits very interesting adsorption properties toward Pb(II) ions in high ionic strength solutions. The ionic strength affects the electrical double layer in an aqueous solution in contact with GO or GO-$C_{60}(OH)_{22}$; therefore, it can strongly influence the Pb(II) uptake. As shown in Fig. 2f, the adsorption of Pb(II) ions on unmodified GO slightly decreases at an ionic strength of 0.001–0.1 mol L^{-1}. This effect is typical for the adsorption of Pb(II) ions on GO from the solution of such low ionic strength at pH < 7 [67,68]. At higher ionic strength, the adsorption of Pb(II) ions on GO decreases quickly and reaches a value close to zero at 5 mol L^{-1}. GO-$C_{60}(OH)_{22}$ is much more resistant to ionic strength, i.e., the adsorption of Pb(II) ions is close to 100% at ionic strength up to 1 mol L^{-1} and then decreases slowly. According to the surface complexation triple-layer model, the inner-sphere complexes are less impressionable to ionic strength variations than outer-sphere surface complexes [69]. Therefore, the effect of ionic strength suggests that an inner-sphere model based on surface complexation is the main mechanism of adsorption of Pb(II) ions on GO-$C_{60}(OH)_{22}$. The effect of ionic strength shows that 460 000-fold excess of Na^+ and 1 240 000-fold excess of NO_3^- do not influence the adsorption of Pb(II) ions. The experiment also shows that other coexisting ions, both anions and cations (Table 3) at very high concentrations (from 20 000 to 100 000-fold excess), practically do not affect Pb(II) uptake. The lower excess of Hg (II) ions, in this experiment, results from their precipitation at pH 5.5 and concentrations higher than 0.05 mg mL^{-1}.

Experiment on coexisting ions suggests that Pb(II) form more stable complexes with fullerenol molecules at pH 5.5 than other metals. The above experiments show a tremendously high affinity of Pb ions toward GO-$C_{60}(OH)_{22}$ at pH 5.5, thus in this instance, the elution and reusability tests were conducted to study its potential use in water purification. According to Fig. 2g, it is possible to elute the Pb(II) using low concentrated 0.1 M HNO_3, therefore allowing to reduce the consumption of more concentrated eluents in the view of its more comprehensive application and greenness. The results prove that the proposed nanomaterial can be reused up to 7 times without losing its maximum adsorption capacity. Compared to other GO-based adsorbents (Table 4), GO-$C_{60}(OH)_{22}$ exhibits very interesting adsorption properties (i.a., high adsorption capacity, high selectivity, short adsorption time with

Table 3
Effect of coexisting ions (concentration of Pb(II) ions equals 25 ng mL^{-1}).

Coexisting ion	Concentration of coexisting ion, mg mL^{-1}	Excess of coexisting ion	Adsorption of Pb (II) ions (%)
NO_3^-	2.5	100,000	101.0 ± 1.1
Cl^-	2.5	100,000	99.5 ± 0.4
PO_4^{3-}	1.0	40,000	99.4 ± 1.9
SO_4^{2-}	2.5	100,000	102.2 ± 1.9
Na^+	2.5	100,000	100.1 ± 1.2
K^+	2.5	100,000	102.2 ± 1.7
Mg^{2+}	1.75	70,000	99.5 ± 2.7
Ca^{2+}	1.25	50,000	99.4 ± 1.0
Al^{3+}	0.5	20,000	97.4 ± 0.9
Mn^{2+}	2.5	100,000	100.5 ± 2.6
Fe^{3+}	0.5	20,000	98.2 ± 1.4
Co^{2+}	1.5	60,000	98.2 ± 1.2
Ni^{2+}	1.5	60,000	99.4 ± 1.2
Cu^{2+}	0.5	20,000	100.6 ± 2.9
Zn^{2+}	0.75	30,000	98.0 ± 2.0
Cd^{2+}	2.5	100,000	100.3 ± 1.1
Hg^{2+}	0.05	2000	100.2 ± 2.6

Table 4
Recently published GO-based materials for adsorption of Pb(II) ions.

Adsorbent	pH	Contact time, min	Dosage, mg L^{-1}	Capacity, mg g^{-1}	Ref.
GO	6.0		100	842	[67]
GO	5.0	15–60	100	1119	[70]
GO	5.5	20–80	1000	987	[71]
GO-EDTA	6.8	20	125	479	[72]
GO/$MnFe_2O_4$	6.0	30	160	621	[73]
GO/Fe_3O_4	6.0	10	100	777	[74]
GO/Fe_3O_4-EDTA	6.8	50	500	211	[75]
GO/Fe_3O_4/CS	5.0	420	1000	112	[76]
GO/Fe_3O_4/CS/EDTA	8.0	22	190	667	[77]
GO/SA-PAM	5.5	60	500	241	[78]
GO-$C_{60}(OH)_{22}$	5.5	30	5	1307	This work
	5.5	<5	10		

EDTA - ethylenediamine triacetic (or tetraacetic) acid, CS - chitosan, SA-PAM - sodium alginate grafted polyacrylamide

minimal adsorbent dose) and may find potential water treatment applications, also in the determination of Pb(II) at ultratrace level in water samples (exceptionally highly saline samples and in the presence of complex matrix). In summary, if the initial pH of the water to be treated is different from 5.5, then the pH should be adjusted to this value first, and at least 10 mg of GO-$C_{60}(OH)_{22}$ per liter of water should be used if a rapid adsorption process is required. If not, then a smaller adsorbent dose can be applied.

The isotherms, kinetics, and effect of ionic strength suggest that the adsorption of Pb(II) ions on GO-$C_{60}(OH)_{22}$ is based on chemisorption, i.e., the chelation of Pb(II) ions by deprotonated hydroxyl groups, and can be described by the inner-sphere model. The chelation of Pb(II) ions by hydroxyl groups was also confirmed by XPS measurements. Fig. 3 shows the high-resolution O1s and Pb4f spectra of GO-$C_{60}(OH)_{22}$ before and after Pb(II) ions adsorption. As previously written, the O1s spectrum of GO-$C_{60}(OH)_{22}$ was deconvoluted into three peaks at 531.3, 532.8, and 534.2 eV assigned to C═O (carboxyl and carbonyl groups), C-OH/C-O-C (hydroxyl and epoxy groups), and H_2O/C-OH (carboxyl group), respectively. After Pb(II) uptake, the O1s spectrum is widened and shifted to the higher binding energy. The most interesting is the presence of two intense peaks at 533.7 and 535.1 eV. The shift to higher energy confirms that the hydroxyl groups are involved in the Pb(II) adsorption [41,79]. Two peaks can suggest the various coordination of Pb(II) ions to the oxygen functional groups. The water molecules physically adsorbed on GO-$C_{60}(OH)_{22}$ and coordinated to the Pb(II) ions can also contribute to these peaks. As shown in Fig. 3, the high-resolution Pb4f spectrum of GO-$C_{60}(OH)_{22}$ after adsorption of Pb(II) ions was deconvoluted into three doublets corresponding to $4f_{7/2}$ and $4f_{5/2}$ levels. The peak at 139.1 eV can be assigned to $Pb(NO_3)_2$ [80,81] (for comparison, O1s and Pb4f spectra are shown for a solid $Pb(NO_3)_2$, which was used in the adsorption experiment). Pb4f spectrum reveals intensive peak at 139.2 eV assigned to $Pb(NO_3)_2$, and two additional peaks at 136.2 and 138.0 eV, which correspond to some surface defects and surface impurities, i.e., Pb$(CO_3)_2$/$Pb(OH)_2$. The O1s spectrum of solid $Pb(NO_3)_2$ shows the intensive peak at 532.7 eV assigned to $Pb(NO_3)_2$ and two small peaks at 529.3 and 531.1 eV, which correspond to some surface impurities, i.e., PbO and Pb$(CO_3)_2$/$Pb(OH)_2$, respectively) [80,82,83]. It should be emphasized that the presence of $Pb(NO_3)_2$ in GO-$C_{60}(OH)_{22}$ results from the preparation of the sample for XPS measurements (after the adsorption of Pb(II) ions, the adsorbent is separated and dried). In an aqueous solution, according to the surface complexation triple-layer model, the following nitrate complexes are possible: GO-$C_{60}(OH)_{21}O^-\cdots PbNO_3^+$ (outer-sphere), GO-$C_{60}(OH)_{21}O\text{-}Pb^+\cdots NO_3^-$ (ion pair of nitrate with inner-sphere Pb), GO-$C_{60}(OH)_{21}O\text{-}Pb\text{-}NO_3$ (inner-sphere Pb nitrate surface complex) [69]. Aside from the presence of nitrate complexes, the most interesting in the Pb4f spectrum is the presence of two intense peaks at 141.2 and 142.6 eV. These binding energies are higher than those reported for Pb(II) coordinated by oxygen-functional groups of biochar (138.6–139.5 eV) [84,85], GO (138.2–138.8 eV) [86–88], β-cyclodextrin (138.4 eV) [89], oxidized-CNTs (139.3 eV) [90,91]. It suggests the strong complexation of Pb(II) ions by fullerenol molecules. Moreover, the presence of two peaks suggests the various coordination of Pb(II) ions to the oxygen functional groups.

3.3. GO-$C_{60}(OH)_{22}$ in ultrasensitive determination of Pb(II) using TXRF

Huge adsorption capacity, impressive selectivity toward Pb(II) ions, and excellent dispersibility in aqueous solutions make it possible to use GO-$C_{60}(OH)_{22}$ in micro-quantities and open the path to a simple and ultrasensitive determination of Pb(II) by such micro-analytical technique as TXRF. It is worth emphasized here that properties of GO-$C_{60}(OH)_{22}$ are not only interesting from the view of its adsorptive properties but also TXRF measurement: (a) X-ray characteristic radiation of carbon and oxygen that are the major elements of the adsorbent is not detected by TXRF instruments, (b) the particle size effects can be neglected because of the very small size of GO-$C_{60}(OH)_{22}$ nanoparticles, (c) the flexibility and softness of GO-$C_{60}(OH)_{22}$ nanosheets allow preparing smooth and thin samples deposited onto quartz reflectors what is especially important in the measurement under total reflection conditions. The developed method based on DMSPE consists of dispersing GO-$C_{60}(OH)_{22}$ in the analyzed sample solution and depositing the isolated GO-$C_{60}(OH)_{22}$ with adsorbed Pb(II) ions on the TXRF reflector. Therefore, the adsorbent dose is important for both the adsorption of Pb(II) ions and the TXRF measurement. Accordingly, it is worth noting that the adsorbent dose should be large enough to obtain high adsorption in a short time. On the other hand, the adsorbent dose should be as low as possible to obtain a minimal scattering of primary X-ray radiation and low background in TXRF measurement. The kinetics curves (Fig. 2d and 2e) showed that the high adsorption could be achieved within 30 min using a minimal adsorbent dose of 5 mg L^{-1}. Using this dose of GO-$C_{60}(OH)_{22}$, the sample volume will determine the final amount of adsorbent deposited on the TXRF reflector. In this study, the Pb(II) ions were preconcentrated from the initial sample volume of 100 mL using 500 μg of GO-$C_{60}(OH)_{22}$. Thus, the final amount of GO-$C_{60}(OH)_{22}$ deposited on the reflector is only 10 μg (see Section 2.5) what allows to obtain a very low background of TXRF spectrum and finally extremely low limit of detection (LOD), i.e., 2.3 pg mL^{-1} (calculated from the formula $LOD = (3/k)(R_B/t)^{1/2}$, where k is the method sensitivity in counts s^{-1} mL pg^{-1}, R_B is the count rate of the background in counts s^{-1}, and t is the measurement time in s). The LOD of 2.3 pg mL^{-1} was obtained for the measurement time of 600 s. However, the LOD can be

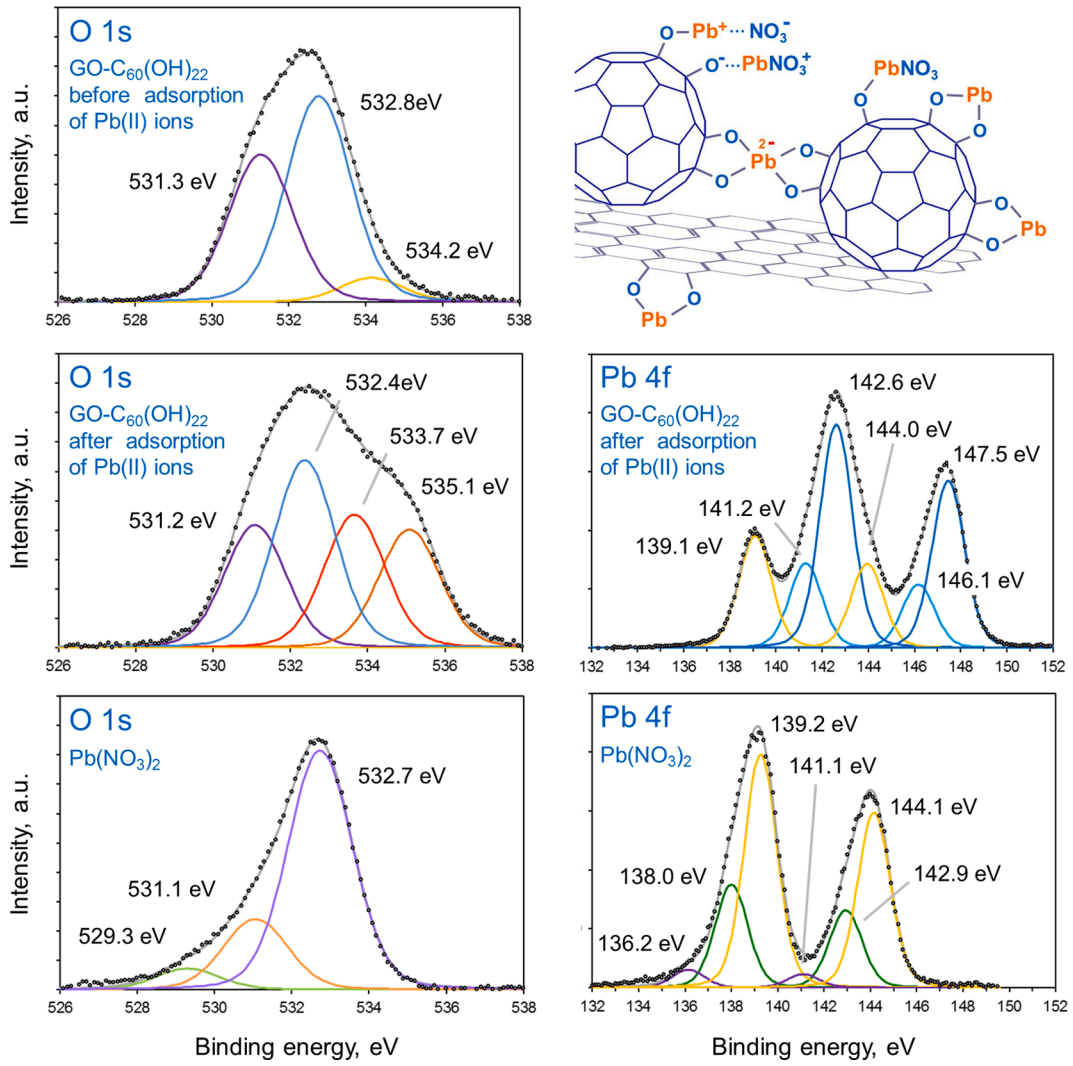

Fig. 3. The high-resolution O1s and Pb4f XPS spectra of $Pb(NO_3)_2$ and GO-$C_{60}(OH)_{22}$ before and after adsorption Pb(II) ions.

lowered to 1.1 pg mL^{-1} by extending the measurement time to 1200 s. Such low LOD was possible to obtain due to the very low background, the high sensitivity of TXRF measurement, and high preconcentration factor (PF) of 200. As shown in Table 5, the LOD is much lower than those obtained by the recently published methods based on FAAS and ICP-OES, or some lower/comparable to ET-AAS and ICP-MS. Due to the impressive selectivity of the DSPME/TXRF method, the ultra-trace Pb(II) ions can be highly accurately determined in complex matrix samples, including high salinity waters challenging to analyze using other analytical techniques. Therefore, the developed method seems very promising, even compared to ET-AAS and ICP-MS, which are considered very sensitive but require analyte isolation from samples with complex matrices, such as in determining lead in seawater.

Table 5
Comparison of performance with other recently published methods for determination of Pb(II) ions.

Technique	Preconcentration/ separation method	PF	RSD, %	LOD, pg mL^{-1}	Ref.
FAAS	DMSPE	50	3	2000	[6]
FAAS	SPE	94	1.2	1200	[7]
ICP-OES	MDSPE	150	3.1	760	[8]
ICP-OES	LLME	150	0.8	200	[9]
ICP-OES	DMSPE	145	3.5	60	[10]
ET-AAS	SPE	16	5.4	320	[11]
ET-AAS	LLME	59	1.0–3.2	25	[12]
ET-AAS	MDSPE	200	3.5	8	[13]
ICP-MS	Co-precipitation	10		8	[14]
ICP-MS	SPME	10	<17	7	[15]
ICP-MS	MDSPE	150	8	2.9	[16]
TXRF	DMSPE	200	4.1	2.3	This work

The high sensitivity of the DMSPE/TXRF procedure is visualized in Fig. 4a and 4b, which show TXRF spectra of river and lake water samples before and after preconcentration of Pb(II) ions (initial sample volume 100 mL, PF = 200). If such a low LOD as 2.3 pg mL^{-1} is not required, the preconcentration procedure can be performed using a smaller sample volume. Fig. 4c shows the TXRF spectrum of the spring water sample (NIST 1640a) before and after preconcentration of Pb(II) ions. As can be seen, the procedure allows for preconcentration of Pb(II) ions and the separation of Pb(II) ions from other ions, including interfering arsenic. The separation of Pb(II) ions from the highly saline matrix and the accurate determination of Pb(II) ions in seawater is another example showing the advantages of the developed DMSPE/TXRF method (Fig. 4d). Because of the high concentration of Pb(II) ions in QC3163, the DMSPE/TXRF method was used to separate the analyte from the sample matrix (i.e., sodium chloride). In direct TXRF analysis (without preconcentration or separation step), the seawater was diluted three times before depositing on a quartz reflector to obtain thin, dried residue suitable for TXRF measurement. As shown in Fig. 4d, in the direct TXRF measurement, the Pb intensity is significantly underestimated (even

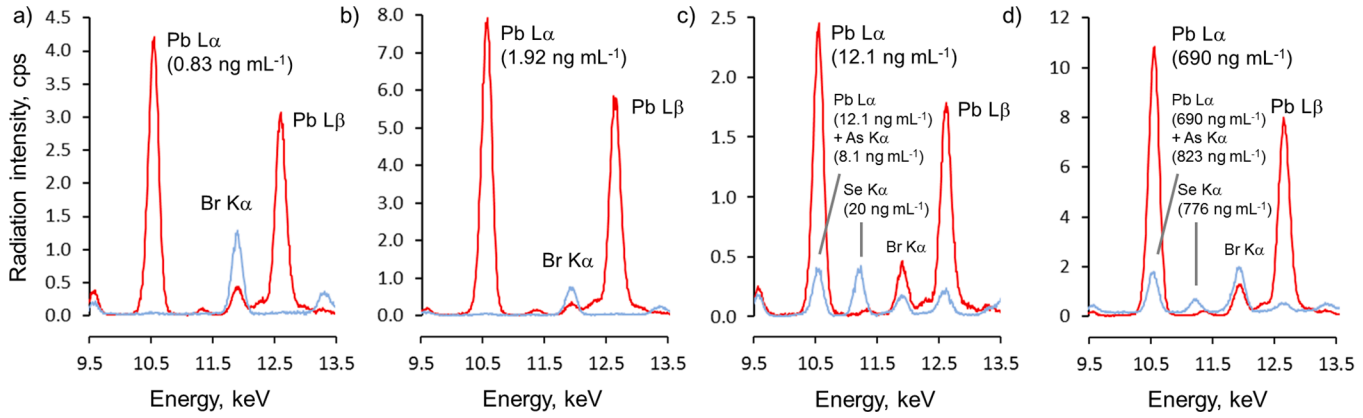

Fig. 4. TXRF spectra of water samples before (blue line) and after preconcentration (red line). Pb(II) ions were preconcentrated/separated from 100 mL (PF = 200) of the river (a) and lake (b) water samples, 5 mL (PF = 10) of NIST 1640a spring water sample (c), and 0.5 mL (PF = 1) of QC3163 seawater sample (d).

taking into account sample dilution) to the radiation intensity after Pb (II) separation. It results from the significant absorption of Pb characteristic radiation by the dried residue (e.g., sodium and magnesium chlorides) [92]. Thus, the accurate results for this sample type can be obtained only after separating Pb(II) ions.

The TXRF quantification of Pb(II) ions was performed using calibration samples prepared by preconcentration of water samples spiked with the known concentration of Pb(II). The calibration graph is based on the plot of the ratio of Pb and Y intensities (I_{Pb} and I_Y) *vs.* Pb concentration (C_{Pb}): $I_{Pb}/I_Y = k_{Pb/Y} \times C_{Pb} + b$. Yttrium is used as the internal standard to correct the non-reproducibility of the GO-$C_{60}(OH)_{22}$ residue position on the TXRF reflector and the inhomogeneous excitation due to the standing-wave field above the reflector surface [92]. Therefore, the ratio I_{Pb}/I_Y does not depend on residue position on the reflector and measurement conditions. The measurement of calibration samples shows the linearity in a very wide range of concentrations from 0.005 to 50 ng mL^{-1}, confirmed by excellent correlation coefficients of 0.9999. The recovery and precision of the method were examined by the analysis of seven water samples spiked with a low concentration of Pb(II), i.e., 0.1 ng mL^{-1}. The results show the quantitative recovery of 101 ± 4.0%. The relative standard deviation (RSD) of 4.0%, which characterizes the total precision of the method, can be considered very good for ultratrace analysis. It should be noted that the precision of the TXRF measurement (0.7%) and the precision of the pipetting suspension on the quartz reflector (1.7%) contribute to this value. The accuracy of the DMSPE/TXRF method was verified by the analysis of certified reference materials (spring water NIST 1640a, groundwater BCR-610, estuarine water LGC 6016, and seawater QC3163) and water samples (river, lake, and mineral water) spiked with the known concentration of Pb(II) ions. The results presented in Table 6 show excellent agreement between TXRF results and certified/spiked concentrations, i.e., recovery in the range 95.0–103.3%, with an average recovery of 100.2%. As mentioned above, these results were achieved using a "classical" calibration graph using an internal standard to correct GO-$C_{60}(OH)_{22}$ residue position on the TXRF reflector. However, TXRF spectrometry makes it possible to use only the internal standard without performing calibration using a series of standard samples. The quantification is based on the net intensities of analyte and internal standard, and the instrumental sensitivities for these elements [92]. The results of this quantification method are included in Table 6. The recoveries are in the range 101.5–108.0%, and the average recovery of Pb(II) equals 104.2%.

Table 6
Determination of Pb(II) in certified and spiked water samples using two quantification approach: calibration graph and only internal standard. The uncertainties correspond to one standard deviation, n = 3.

Sample	Added, ng mL^{-1}	Calibration graph		Internal standard	
		Found, ng mL^{-1}	Recovery (%)	Found, ng mL^{-1}	Recovery (%)
River water	–	0.827 ± 0.013	–	0.81 ± 0.035	–
	1.00	1.86 ± 0.030	103	1.88 ± 0.020	107
Lake water	–	1.92 ± 0.027	–	1.88 ± 0.026	–
	2.00	3.87 ± 0.042	98	3.91 ± 0.010	102
Mineral water	–	0.26 ± 0.011	–	0.249 ± 0.0046	–
	0.20	0.450 ± 0.0022	95	0.452 ± 0.0077	102
Spring water NIST 1640a	12.101 ± 0.050[a]	12.2 ± 0.23	101	12.7 ± 0.24	105
Ground water BCR-610	7.78 ± 0.13[a,b]	8.0 ± 0.33	103	8.4 ± 0.34	108
Estuarine water LGC 6016	196 ± 3[a,b]	200.0 ± 0.57	102	205.2 ± 0.58	105
Sea water QC3163	690 ± 12.3[a]	687 ± 5.1	100	704 ± 4.9	102

[a] Certified concentration
[b] certified concentration in ng g^{-1}

4. Conclusions

The fullerenol nanoparticles are highly soluble in aqueous solutions, and due to the deprotonation, they can react with metal ions to produce insoluble metal-fullerenol cross-linked polymers. However, the fullerenol nanoparticles remain soluble in water if the concentration of metal ions is very low. Thus, the application of pure fullerenol in trace or ultra-trace separation is limited. In this paper, the fullerenol nanoparticles were grafted to the surface of GO what solves the problem of their high solubility and simultaneously uses their high hydrophilicity and deprotonation ability. The research has revealed unique adsorption properties of GO-$C_{60}(OH)_{22}$ toward Pb(II) ions, i.e. enormous adsorption capacity (1307 mg g^{-1}) and selectivity, much higher than those of any of the currently reported sorbents, including GO and its derivatives. The isotherms, kinetics, and effect of ionic strength suggest that the adsorption of Pb(II) ions on GO-$C_{60}(OH)_{22}$ is based on chemisorption and can be described by the inner-sphere model. The high-resolution XPS spectroscopy confirms the strong chelation of Pb(II) ions and suggests the various coordination of Pb(II) ions to the oxygen functional groups. The exceptional properties of GO-$C_{60}(OH)_{22}$, including the possibility of application in micro-quantities, allow for the development of the method for ultra-sensitive determination of Pb(II) ions by TXRF using a simplified approach based only on the internal standard. The

method allows obtaining an extremely low LOD at the ppt levels using a low-power TXRF instrument with no gas consumption. It is also noteworthy that LOD is ca. 4000–6000 times lower than the guideline value and maximum contaminant level of a lead according to WHO or EPA regulations [5,93]. Besides, obtained LOD is much lower or at least comparable to the most common analytical methods favorably used in Pb(II) determination. Over and above that, the proposed ultra-selective DMSPE/TXRF procedure proves itself thoroughly in the accurate determination of Pb(II) ions in the samples of a complex matrix, high salinity, or both, which is impossible with the use of other techniques, especially highly sensitive ICP-MS or ET-AAS, complicating and lengthening the sample preparation stage in order to isolate lead ions.

CRediT authorship contribution statement

Rafal Sitko: Conceptualization, Methodology, Writing – original draft. **Marcin Musielak:** Methodology, Writing – original draft, Investigation, Validation. **Maciej Serda:** Investigation, Writing – review & editing. **Ewa Talik:** Investigation. **Anna Gagor:** Investigation. **Beata Zawisza:** Validation, Writing – review & editing. **Malgorzata Malecka:** Investigation.

Declaration of Competing Interest

The authors declare that they have no known competing financial interests or personal relationships that could have appeared to influence the work reported in this paper.

Acknowledgements

The project was supported by the National Science Centre (Poland) by the Grant No. 2018/31/B/ST4/00041.

References

[1] C. Xiong, S. Wang, P. Hu, L. Huang, C. Xue, Z. Yang, X. Zhou, Y. Wang, H. Ji, Efficient selective removal of Pb(II) by using 6-Aminothiouracil-modified zr-based organic frameworks: From experiments to mechanisms, ACS Appl. Mater. Interfaces. 12 (2020) 7162–7178, https://doi.org/10.1021/acsami.9b19516.
[2] R. Deng, D. Huang, L. Lei, C. Zhou, L. Yin, X. Liu, S. Chen, R. Li, J. Tao, Stabilization of lead in polluted sediment based on an eco-friendly amendment strategy: Microenvironment response mechanism, J. Hazard. Mater. 415 (2021), 125534, https://doi.org/10.1016/j.jhazmat.2021.125534.
[3] S.T. Shefa, P. Héroux, Both physiology and epidemiology support zero tolerable blood lead levels, Toxicol. Lett. 280 (2017) 232–237, https://doi.org/10.1016/j.toxlet.2017.08.015.
[4] J. Nie, Q. Wang, S. Gao, C.S. Poon, Y. Zhou, J. shan Li, Novel recycling of incinerated sewage sludge ash (ISSA) and waste bentonite as ceramsite for Pb-containing wastewater treatment: Performance and mechanism, J. Environ. Manage. 288 (2021), 112382, https://doi.org/10.1016/j.jenvman.2021.112382.
[5] Environmental Protection Agency, National Primary Drinking Water Regulations, (2009). https://www.epa.gov/ground-water-and-drinking-water/national-primary-drinking-water-regulations#one (accessed June 28, 2021).
[6] M. Abdolhosseini, F. Shemirani, S.M. Yousefi, Poly (deep eutectic solvents) as a new class of sustainable sorbents for solid phase extraction: application for preconcentration of Pb (II) from food and water samples, Microchim. Acta. 187 (2020) 602, https://doi.org/10.1007/s00604-020-04564-5.
[7] S. Bajaj, V. Jain, N. Sharma, S. Tiwari, R. Saxena, Efficient lead preconcentration using two chemically functionalized carbon nanotubes in hyphenated flow injection-flame atomic absorption spectrometry system, J. Chromatogr. A. 1638 (2021), 461888, https://doi.org/10.1016/j.chroma.2021.461888.
[8] N. Kobylinska, L. Kostenko, S. Khainakov, S. Garcia-Granda, Advanced core-shell EDTA-functionalized magnetite nanoparticles for rapid and efficient magnetic solid phase extraction of heavy metals from water samples prior to the multi-element determination by ICP-OES, Microchim. Acta. 187 (2020) 1–15, https://doi.org/10.1007/s00604-020-04231-9.
[9] S.V. Smirnova, D.V. Ilin, I.V. Pletnev, Extraction and ICP-OES determination of heavy metals using tetrabutylammonium bromide aqueous biphasic system and oleophilic collector, Talanta. 221 (2021), 121485, https://doi.org/10.1016/j.talanta.2020.121485.
[10] L. Nyaba, P.N. Nomngongo, Determination of trace metals in vegetables and water samples using dispersive ultrasound-assisted cloud point-dispersive μ-solid phase extraction coupled with inductively coupled plasma optical emission spectrometry, Food Chem. 322 (2020), 126749, https://doi.org/10.1016/j.foodchem.2020.126749.
[11] W.T. Li, Z.J. Hu, J. Meng, X. Zhang, W. Gao, M.L. Chen, J.H. Wang, Zn-based metal organic framework-covalent organic framework composites for trace lead extraction and fluorescence detection of TNP, J. Hazard. Mater. 411 (2021), 125021, https://doi.org/10.1016/j.jhazmat.2020.125021.
[12] P. Chaikhan, Y. Udnan, R.J. Ampiah-Bonney, W.C. Chaiyasith, Air-assisted solvent terminated dispersive liquid–liquid microextraction (AA-ST-DLLME) for the determination of lead in water and beverage samples by graphite furnace atomic absorption spectrometry, Microchem. J. 162 (2021), 105828, https://doi.org/10.1016/j.microc.2020.105828.
[13] P. Montoro-Leal, J.C. García-Mesa, M.T. Siles Cordero, M.M. López Guerrero, E. Vereda Alonso, Magnetic dispersive solid phase extraction for simultaneous enrichment of cadmium and lead in environmental water samples, Microchem. J. 155 (2020), 104796, https://doi.org/10.1016/j.microc.2020.104796.
[14] Z. Arslan, T. Oymak, J. White, Triethylamine-assisted Mg(OH)2 coprecipitation/preconcentration for determination of trace metals and rare earth elements in seawater by inductively coupled plasma mass spectrometry (ICP-MS), Anal. Chim. Acta. 1008 (2018) 18–28, https://doi.org/10.1016/j.aca.2018.01.017.
[15] J. jun Fei, L. yu Zhao, X. hong Wu, X. bing Cui, H. Min, H. zhen Lian, Y. jun Chen, In-tube solid-phase microextraction with a hybrid monolithic column for the preconcentration of ultra-trace metals prior to simultaneous determination by ICP-MS, Microchim. Acta. 187 (2020) 356, https://doi.org/10.1007/s00604-020-04329-0.
[16] Y. Chen, M. He, B. Chen, B. Hu, Thiol-grafted magnetic polymer for preconcentration of Cd, Hg, Pb from environmental water followed by inductively coupled plasma mass spectrometry detection, Spectrochim, Acta - Part B At. Spectrosc. 177 (2021), 106071, https://doi.org/10.1016/j.sab.2021.106071.
[17] R. Baby, B. Saifullah, M.Z. Hussein, Carbon nanomaterials for the treatment of heavy metal-contaminated water and environmental remediation, Nanoscale Res. Lett. 14 (2019) 1–17, https://doi.org/10.1186/s11671-019-3167-8.
[18] X. Liu, R. Ma, X. Wang, Y. Ma, Y. Yang, L. Zhuang, S. Zhang, R. Jehan, J. Chen, X. Wang, Graphene oxide-based materials for efficient removal of heavy metal ions from aqueous solution: A review, Environ. Pollut. 252 (2019) 62–73, https://doi.org/10.1016/j.envpol.2019.05.050.
[19] X. Yang, Y. Wan, Y. Zheng, F. He, Z. Yu, J. Huang, H. Wang, Y.S. Ok, Y. Jiang, B. Gao, Surface functional groups of carbon-based adsorbents and their roles in the removal of heavy metals from aqueous solutions: A critical review, Chem. Eng. J. 366 (2019) 608–621, https://doi.org/10.1016/j.cej.2019.02.119.
[20] J.Y. Lim, N.M. Mubarak, E.C. Abdullah, S. Nizamuddin, M. Khalid, Inamuddin, Recent trends in the synthesis of graphene and graphene oxide based nanomaterials for removal of heavy metals — A review, J. Ind. Eng. Chem. 66 (2018) 29–44, https://doi.org/10.1016/j.jiec.2018.05.028.
[21] J. Xu, Z. Cao, Y. Zhang, Z. Yuan, Z. Lou, X. Xu, X. Wang, A review of functionalized carbon nanotubes and graphene for heavy metal adsorption from water: Preparation, application, and mechanism, Chemosphere. 195 (2018) 351–364, https://doi.org/10.1016/j.chemosphere.2017.12.061.
[22] M. Ghorbani, O. Seyedin, M. Aghamohammadhassan, Adsorptive removal of lead (II) ion from water and wastewater media using carbon-based nanomaterials as unique sorbents: A review, J. Environ. Manage. 254 (2020), 109814, https://doi.org/10.1016/j.jenvman.2019.109814.
[23] J. Chawla, R. Kumar, I. Kaur, Carbon nanotubes and graphenes as adsorbents for adsorption of lead ions from water: a review, J. Water Supply Res. Technol. - AQUA. 64 (2015) 641–659, https://doi.org/10.2166/aqua.2015.102.
[24] H.W. Kroto, J.R. Heath, S.C. O'Brien, R.F. Curl, R.E. Smalley, C60: Buckminsterfullerene, Nature. 318 (1985) 162–163, https://doi.org/10.1038/318162a0.
[25] M. Valcárcel, S. Cárdenas, B.M. Simonet, Y. Moliner-Martínez, R. Lucena, Carbon nanostructures as sorbent materials in analytical processes, TrAC - Trends Anal. Chem. 27 (2008) 34–43, https://doi.org/10.1016/j.trac.2007.10.012.
[26] J. Muñoz, M. Gallego, M. Valcárcel, Solid-phase extraction-gas chromatography-mass spectrometry using a fullerene sorbent for the determination of inorganic mercury(II), methylmercury(I) and ethylmercury(I) in surface waters at sub-ng/ml levels, J. Chromatogr. A. 1055 (2004) 185–190, https://doi.org/10.1016/j.chroma.2004.09.026.
[27] J. Muñoz, M. Gallego, M. Valcárcel, Speciation analysis of mercury and tin compounds in water and sediments by gas chromatography-mass spectrometry following preconcentration on C60 fullerene, Anal. Chim. Acta. 548 (2005) 66–72, https://doi.org/10.1016/j.aca.2005.05.062.
[28] M.G. Pereira, E.R. Pereira-Filho, H. Berndt, M.A.Z. Arruda, Determination of cadmium and lead at low levels by using preconcentration at fullerene coupled to thermospray flame furnace atomic absorption spectrometry, Spectrochim, Acta - Part B At. Spectrosc. 59 (2004) 515–521, https://doi.org/10.1016/j.sab.2003.12.012.
[29] J.R. Baena, S. Cárdenas, M. Gallego, M. Valcárcel, Speciation of inorganic lead and ionic alkyllead compounds by GC/MS in prescreened rainwaters, Anal. Chem. 72 (2000) 1510–1517, https://doi.org/10.1021/ac9911903.
[30] A. Djordjevic, B. Srdjenovic, M. Seke, D. Petrovic, R. Injac, J. Mrdjanovic, Review of synthesis and antioxidant potential of fullerenol nanoparticles, J. Nanomater. 2015 (2015) 1–15, https://doi.org/10.1155/2015/567073.
[31] A. Kraft, P. Roth, D. Schmidt, J. Stangl, K. Müller-Buschbaum, F. Beuerle, Three-Dimensional Metal-Fullerene Frameworks, Chem. - A Eur. J. 22 (2016) 5982–5987, https://doi.org/10.1002/chem.201505137.
[32] F. Leng, I.C. Gerber, P. Lecante, A. Bentaleb, A. Muñoz, B.M. Illescas, N. Martín, G. Melinte, O. Ersen, H. Martinez, M.R. Axet, P. Serp, Hexakis [60]Fullerene Adduct-Mediated Covalent Assembly of Ruthenium Nanoparticles and Their Catalytic Properties, Chem. - A Eur. J. 23 (2017) 13379–21338, https://doi.org/10.1002/chem.201701043.

[33] M.D. Meijer, G.P.M. Van Klink, G. Van Koten, Metal-chelating capacities attached to fullerenes, Coord. Chem. Rev. 230 (2002) 141–163, https://doi.org/10.1016/s0010-8545(01)00456-8.
[34] L.Y. Chiang, J.W. Swirczewski, C.S. Hsu, S.K. Chowdhury, S. Cameron, K. Creegan, Multi-hydroxy additions onto C60 fullerene molecules, J. Chem. Soc. Chem. Commun. (1992) 10154–10157, https://doi.org/10.1039/C39920001791.
[35] L.Y. Chiang, R.B. Upasani, J.W. Swirczewski, Versatile Nitronium Chemistry for C60 Fullerene Functionalization, J. Am. Chem. Soc. 114 (1992) 10154–10157, https://doi.org/10.1021/ja00052a010.
[36] J. Li, A. Takeuchi, M. Ozawa, X. Li, K. Saigo, K. Kitazawa, C60 fullerol formation catalysed by quaternary ammonium hydroxides, J. Chem. Soc. Chem. Commun. 8 (1993) 1784–1785, https://doi.org/10.1039/C39930001784.
[37] K. Kokubo, K. Matsubayashi, H. Tategaki, H. Takada, T. Oshima, Facile synthesis of highly water-soluble fullerenes more than half-covered by hydroxyl groups, ACS Nano. 2 (2008) 327–333, https://doi.org/10.1021/nn700151z.
[38] K.N. Semenov, N.A. Charykov, V.N. Keskinov, Fullerenol synthesis and identification. properties of the fullerenol water solutions, J. Chem. Eng. Data. 56 (2011) 230–239, https://doi.org/10.1021/je100755v.
[39] S. Assemi, S. Tadjiki, B.C. Donose, A.V. Nguyen, J.D. Miller, Aggregation of fullerol $C_{60}(OH)_{24}$ nanoparticles as revealed using flow field-flow fractionation and atomic force microscopy, Langmuir. 26 (2010) 16063–16070, https://doi.org/10.1021/la102942b.
[40] J.A. Brant, J. Labille, C.O. Robichaud, M. Wiesner, Fullerol cluster formation in aqueous solutions: Implications for environmental release, J. Colloid Interface Sci. 314 (2007) 281–288, https://doi.org/10.1016/j.jcis.2007.05.020.
[41] R. Anderson, A.R. Barron, Reaction of hydroxyfullerene with metal salts: A route to remediation and immobilization, J. Am. Chem. Soc. 127 (2005) 10458–10459, https://doi.org/10.1021/ja051659d.
[42] J. Heimann, L. Morrow, R.E. Anderson, A.R. Barron, Understanding the relative binding ability of hydroxyfullerene to divalent and trivalent metals, Dalt. Trans. 44 (2015) 4380–4388, https://doi.org/10.1039/c4dt03376k.
[43] D.C. Marcano, D.V. Kosynkin, J.M. Berlin, A. Sinitskii, Z. Sun, A. Slesarev, L. B. Alemany, W. Lu, J.M. Tour, Improved synthesis of graphene oxide, ACS Nano. 4 (2010) 4806–4814, https://doi.org/10.1021/nn1006368.
[44] M. Musielak, A. Gagor, B. Zawisza, E. Talik, R. Sitko, Graphene oxide/carbon nanotube membranes for highly efficient removal of metal ions from water, ACS Appl. Mater. Interfaces. 11 (2019) 28582–28590, https://doi.org/10.1021/acsami.9b11214.
[45] A. Gholampour, M. Valizadeh Kiamahalleh, D.N.H. Tran, T. Ozbakkaloglu, D. Losic, From graphene oxide to reduced graphene oxide: Impact on the physiochemical and mechanical properties of graphene-cement composites, ACS Appl, Mater. Interfaces. 9 (2017) 43275–43286, https://doi.org/10.1021/acsami.7b16736.
[46] T. Szabó, O. Berkesi, I. Dékány, DRIFT study of deuterium-exchanged graphite oxide, Carbon N. Y. 43 (2005) 3186–3189, https://doi.org/10.1016/j.carbon.2005.07.013.
[47] M. Acik, G. Lee, C. Mattevi, A. Pirkle, R.M. Wallace, M. Chhowalla, K. Cho, Y. Chabal, The role of oxygen during thermal reduction of graphene oxide studied by infrared absorption spectroscopy, J. Phys. Chem. C. 115 (2011) 19761–19781, https://doi.org/10.1021/jp2052618.
[48] A. Bagri, C. Mattevi, M. Acik, Y.J. Chabal, M. Chhowalla, V.B. Shenoy, Structural evolution during the reduction of chemically derived graphene oxide, Nat. Chem. 2 (2010) 581–587, https://doi.org/10.1038/nchem.686.
[49] P. Scharff, C. Siegmund, K. Risch, I. Lysko, O. Lysko, D. Zherebetskyy, A. Ivanisik, A. Gorchinskiy, E. Buzaneva, Characterization of water-soluble fullerene C60 oxygen and hydroxyl group derivatives for photosensitizers, Fullerenes Nanotub. Carbon Nanostructures. 13 (2005) 497–509, https://doi.org/10.1081/FST-200039472.
[50] G. Xing, J. Zhang, Y. Zhao, J. Tang, B. Zhang, X. Gao, H. Yuan, L. Qu, W. Cao, Z. Chai, K. Ibrahim, R. Su, Influences of structural properties on stability of fullerenols, J. Phys. Chem. B. 108 (2004) 11473–11479, https://doi.org/10.1021/jp0487962.
[51] G.C. Alves, L.O. Ladeira, A. Righi, K. Krambrock, H.D. Calado, R.P. De Freitas Gilb, M.V.B. Pinheiro, Synthesis of $C_{60}(OH)_{18-20}$ in aqueous alkaline solution under O_2-atmosphere, J. Braz. Chem. Soc. 17 (2006) 1186–1190, https://doi.org/10.1590/S0103-50532006000600017.
[52] L.O. Husebo, B. Sitharaman, K. Furukawa, T. Kato, L.J. Wilson, Fullerenols revisited as stable radical anions, J. Am. Chem. Soc. 126 (2004) 12055–12064, https://doi.org/10.1021/ja047593o.
[53] J. Wu, L.B. Alemany, W. Li, D. Benoit, J.D. Fortner, Photoenhanced transformation of hydroxylated fullerene (fullerol) by free chlorine in water, Environ. Sci. Nano. 4 (2017) 470–479, https://doi.org/10.1039/c6en00381h.
[54] B. Vileno, P.R. Marcoux, M. Lekka, A. Sienkiewicz, T. Fehér, L. Forró, Spectroscopic and photophysical properties of a highly derivatized C60 fullerol, Adv. Funct. Mater. 16 (2006) 120–128, https://doi.org/10.1002/adfm.200500425.
[55] R. Jaiswal, U. Saha, T.H. Goswami, A. Srivastava, N.E. Prasad, 'Pillar effect' of chemically bonded fullerene in enhancing supercapacitance performances of partially reduced fullerenol graphene oxide hybrid electrode material, Electrochim. Acta. 283 (2018) 269–290, https://doi.org/10.1016/j.electacta.2018.06.110.
[56] P.G. Rouxhet, M.J. Genet, XPS analysis of bio-organic systems, Surf. Interface Anal. 43 (2011) 1453–1470, https://doi.org/10.1002/sia.3831.
[57] D. Hulicova-Jurcakova, M. Seredych, G.Q. Lu, T.J. Bandosz, Combined effect of nitrogen- and oxygen-containing functional groups of microporous activated carbon on its electrochemical performance in supercapacitors, Adv. Funct. Mater. 19 (2009) 438–447, https://doi.org/10.1002/adfm.200801236.
[58] X. Fan, C. Yu, J. Yang, Z. Ling, J. Qiu, Hydrothermal synthesis and activation of graphene-incorporated nitrogen-rich carbon composite for high-performance supercapacitors, Carbon N. Y. 70 (2014) 130–141, https://doi.org/10.1016/j.carbon.2013.12.081.
[59] I. Langmuir, The constitution and fundamental properties of solids and liquids. Part I. Solids, J. Am. Chem. Soc. 38 (1916) 2221–2295, https://doi.org/10.1021/ja02268a002.
[60] I. Langmuir, The adsorption of gases on plane surfaces of glass, mica and platinum, J. Am. Chem. Soc. 40 (1918) 1361–1403, https://doi.org/10.1021/ja02242a004.
[61] H. Freundlich, Über Die Absorption in Lösungen, Zeitschrift Für Phys. Chemie. 57 (1906) 385–470.
[62] Y.S. Elovich, O.G. Larinov, Theory of adsorption from solutions of non electrolytes on solid (I) equation adsorption from solutions and the analysis of its simplest form, (II) verification of the equation of adsorption isotherm from solutions, Izv. Akad. Nauk. SSSR, Otd. Khimicheskikh Nauk. 2 (1962) 209–216.
[63] M.I. Temkin, Adsorption equilibrium and the kinetics of processes on nonhomogeneous surfaces and in the interaction between adsorbed molecules, J. Phys. Chem. 15 (1941) 296–332.
[64] K.R. Hall, L.C. Eagleton, A. Acrivos, T. Vermeulen, Pore- and solid-diffusion kinetics in fixed-bed adsorption under constant-pattern conditions, Ind. Eng. Chem. Fundam. 5 (1966) 212–223, https://doi.org/10.1021/i160018a011.
[65] Y.S.S. Ho, G. McKay, Pseudo-second order model for sorption processes, Process Biochem. 34 (1999) 451–465, https://doi.org/10.1016/S0032-9592(98)00112-5.
[66] S.Y. Lagergren, Zur Theorie der sogenannten Adsorption gel¨oster Stoffe, Kungliga Svenska Vetenskapsakad, Handlingar. 24 (1898) 1–39.
[67] G. Zhao, X. Ren, X. Gao, X. Tan, J. Li, C. Chen, Y. Huang, X. Wang, Removal of Pb (ii) ions from aqueous solutions on few-layered graphene oxide nanosheets, Dalt. Trans. 40 (2011) 10945–10952, https://doi.org/10.1039/c1dt11005e.
[68] X. Li, K. Zhao, C. You, H. Pan, X. Tang, Y. Fang, Impact of contact time, pH, ionic strength, soil humic substances, and temperature on the uptake of Pb(II) onto graphene oxide, Sep. Sci. Technol. 52 (2017) 987–996, https://doi.org/10.1080/01496395.2017.1281302.
[69] K.F. Hayes, J.O. Leckie, Modeling ionic strength effects on cation adsorption at hydrous oxide/solution interfaces, J. Colloid Interface Sci. 115 (1987) 564–572, https://doi.org/10.1016/0021-9797(87)90078-6.
[70] R. Sitko, E. Turek, B. Zawisza, E. Malicka, E. Talik, J. Heimann, A. Gagor, B. Feist, R. Wrzalik, Adsorption of divalent metal ions from aqueous solutions using graphene oxide, Dalt. Trans. 42 (2013) 5682–5689, https://doi.org/10.1039/c3dt33097d.
[71] C.A. Guerrero-Fajardo, L. Giraldo, J.C. Moreno-Pirajáan, Preparation and characterization of graphene oxide for Pb(II) and Zn(II) ions adsorption from aqueous solution: Experimental, thermodynamic and kinetic study, Nanomaterials. 10 (2020) 1022, https://doi.org/10.3390/nano10061022.
[72] C.J. Madadrang, H.Y. Kim, G. Gao, N. Wang, J. Zhu, H. Feng, M. Gorring, M. L. Kasner, S. Hou, Adsorption behavior of EDTA-graphene oxide for Pb(II) removal, ACS Appl. Mater. Interfaces. 4 (2012) 1186–1193, https://doi.org/10.1021/am201645g.
[73] M. Verma, A. Kumar, K.P. Singh, R. Kumar, V. Kumar, C.M. Srivastava, V. Rawat, G. Rao, S. Kumari, P. Sharma, H. Kim, Graphene oxide-manganese ferrite (GO-$MnFe_2O_4$) nanocomposite: One-pot hydrothermal synthesis and its use for adsorptive removal of Pb^{2+} ions from aqueous medium, J. Mol. Liq. 315 (2020), 113769, https://doi.org/10.1016/j.molliq.2020.113769.
[74] T. Guo, C. Bulin, B. Li, Z. Zhao, H. Yu, H. Sun, X. Ge, R. Xing, B. Zhang, Efficient removal of aqueous Pb(II) using partially reduced graphene oxide-Fe_3O_4, Adsorpt. Sci. Technol. 36 (2018) 1031–1048, https://doi.org/10.1177/0263617417744402.
[75] C. Xing, A. Xia, L. Yu, L. Dong, Y. Hao, X. Qi, Enhanced removal of Pb(II) from aqueous solution using EDTA-modified magnetic graphene oxide, Clean - Soil, Air, Water. 49 (2021) 2000272, https://doi.org/10.1002/clen.202000272.
[76] M.S. Samuel, S.S. Shah, J. Bhattacharya, K. Subramaniam, N.D. Pradeep Singh, Adsorption of Pb(II) from aqueous solution using a magnetic chitosan/graphene oxide composite and its toxicity studies, Int. J. Biol. Macromol. 115 (2018) 1142–1150, https://doi.org/10.1016/j.ijbiomac.2018.04.185.
[77] M. Foroughi, M.H.A. Azqhandi, A biological-based adsorbent for a non-biodegradable pollutant: Modeling and optimization of Pb(II) remediation using GO-CS-Fe_3O_4-EDTA nanocomposite, J. Mol. Liq. 318 (2020), 114077, https://doi.org/10.1016/j.molliq.2020.114077.
[78] H. Jiang, Y. Yang, Z. Lin, B. Zhao, J. Wang, J. Xie, A. Zhang, Preparation of a novel bio-adsorbent of sodium alginate grafted polyacrylamide/graphene oxide hydrogel for the adsorption of heavy metal ion, Sci. Total Environ. 744 (2020), 140653, https://doi.org/10.1016/j.scitotenv.2020.140653.
[79] S. Deng, R. Bai, J.P. Chen, Aminated polyacrylonitrile fibers for lead and copper removal, Langmuir. 19 (2003) 5058–5064, https://doi.org/10.1021/la034061x.
[80] H. Abdel-Samad, P.R. Watson, An XPS study of the adsorption of lead on goethite (α-FeOOH), Appl. Surf. Sci. 136 (1998) 46–54, https://doi.org/10.1016/S0169-4332(98)00337-7.
[81] B.L. Zhang, W. Qiu, P.P. Wang, Y.L. Liu, J. Zou, L. Wang, J. Ma, Mechanism study about the adsorption of Pb(II) and Cd(II) with iron-trimesic metal-organic frameworks, Chem. Eng. J. 385 (2020), 123507, https://doi.org/10.1016/j.cej.2019.123507.
[82] Z. Tang, S. Hong, W. Xiao, S. Seal, J. Taylor, Effect of varying blends of finished RO, surface and ground waters on solid lead surfaces, Corros. Sci. 48 (2006) 3413–3427, https://doi.org/10.1016/j.corsci.2006.01.004.
[83] Z. Hua, Y. Lu, X. Tong, D. Feng, X. Xie, Effect of particle size on the surface oxidation and flotation behavior of galena particles in lime system, Sep. Sci.

Technol. 55 (2020) 2987–2993, https://doi.org/10.1080/01496395.2019.1659365.
[84] N. Zhou, H. Chen, J. Xi, D. Yao, Z. Zhou, Y. Tian, X. Lu, Biochars with excellent Pb (II) adsorption property produced from fresh and dehydrated banana peels via hydrothermal carbonization, Bioresour. Technol. 232 (2017) 204–210, https://doi.org/10.1016/j.biortech.2017.01.074.
[85] Y. Chen, Y. Liu, Y. Li, Y. Chen, Y. Wu, H. Li, S. Wang, Z. Peng, R. Xu, Z. Zeng, Novel Magnetic Pomelo Peel Biochar for Enhancing Pb(II) And Cu(II) Adsorption: Performance and Mechanism, Water. Air. Soil Pollut. 231 (2020) 1–15, https://doi.org/10.1007/s11270-020-04788-4.
[86] J. Zheng, L. Xia, S. Song, Electrosorption of Pb(II) in water using graphene oxide-bearing nickel foam as the electrodes, RSC Adv. 7 (2017) 23543–23549, https://doi.org/10.1039/c7ra02956j.
[87] X. Xiao, Q. Wang, G. Owens, F. Chiellini, Z. Chen, Reduced graphene oxide/iron nanoparticles used for the removal of Pb (II) by one step green synthesis, J. Colloid Interface Sci. 557 (2019) 598–607, https://doi.org/10.1016/j.jcis.2019.09.058.
[88] S. Mohan, D.K. Singh, V. Kumar, S.H. Hasan, Modelling of fixed bed column containing graphene oxide decorated by MgO nanocubes as adsorbent for Lead(II) removal from water, J. Water Process Eng. 17 (2017) 216–228, https://doi.org/10.1016/j.jwpe.2017.03.009.
[89] Z. Duan, M. Song, T. Li, S. Liu, X. Xu, R. Qin, C. He, Y. Wang, L. Xu, M. Zhang, Characterization and adsorption properties of cross-linked yeast/β-cyclodextrin polymers for Pb(ii) and Cd(ii) adsorption, RSC Adv. 8 (2018) 31542–31554, https://doi.org/10.1039/c8ra06171h.
[90] H. Wang, A. Zhou, F. Peng, H. Yu, J. Yang, Mechanism study on adsorption of acidified multiwalled carbon nanotubes to Pb(II), J. Colloid Interface Sci. 316 (2007) 277–283, https://doi.org/10.1016/j.jcis.2007.07.075.
[91] J. Zhang, T. Li, X. Li, Y. Liu, N. Li, Y. Wang, X. Li, A key role of inner-cation-π interaction in adsorption of Pb(II) on carbon nanotubes: Experimental and DFT studies, J. Hazard. Mater. 412 (2021), 125187, https://doi.org/10.1016/j.jhazmat.2021.125187.
[92] P. Kregsamer, P. Streli, C. Wobrauschek, Total-Reflection X-ray Fluorescence, in Handbook of X-ray Spectrometry, 2nd ed.,, Marcel Dekker, New York, 2002.
[93] T. Thompson, J. Fawell, S. Kunikane, D. Jackson, S. Appleyard, P. Callan, J. Bartram, P. Kingston, Chemical safety of drinking-water: Assessing priorities for risk management, WHO Library Cataloguing-in-Publication Data, Geneva, 2007.